



**Understanding Transmission Electron Microscopy
Diffraction Patterns Obtained From Infrared
Semiconductor Materials**

by Wendy L. Sarney

ARL-TR-3128

December 2003

NOTICES

Disclaimers

The findings in this report are not to be construed as an official Department of the Army position unless so designated by other authorized documents.

Citation of manufacturer's or trade names does not constitute an official endorsement or approval of the use thereof.

Destroy this report when it is no longer needed. Do not return it to the originator.

Army Research Laboratory

Adelphi, MD 20783-1197

ARL-TR-3128

December 2003

**Understanding Transmission Electron Microscopy
Diffraction Patterns Obtained From Infrared
Semiconductor Materials**

Wendy L. Sarney

Sensors and Electron Devices Directorate, ARL

REPORT DOCUMENTATION PAGE

*Form Approved
OMB No. 0704-0188*

Public reporting burden for this collection of information is estimated to average 1 hour per response, including the time for reviewing instructions, searching existing data sources, gathering and maintaining the data needed, and completing and reviewing the collection information. Send comments regarding this burden estimate or any other aspect of this collection of information, including suggestions for reducing the burden, to Department of Defense, Washington Headquarters Services, Directorate for Information Operations and Reports (0704-0188), 1215 Jefferson Davis Highway, Suite 1204, Arlington, VA 22202-4302. Respondents should be aware that notwithstanding any other provision of law, no person shall be subject to any penalty for failing to comply with a collection of information if it does not display a currently valid OMB control number.

PLEASE DO NOT RETURN YOUR FORM TO THE ABOVE ADDRESS.

1. REPORT DATE (DD-MM-YYYY) December 2003		2. REPORT TYPE Final	3. DATES COVERED (From - To) 01/02-0803	
4. TITLE AND SUBTITLE Understanding Transmission Electron Microscopy Diffraction Patterns Obtained From Infrared Semiconductor Materials			5a. CONTRACT NUMBER	
			5b. GRANT NUMBER	
			5c. PROGRAM ELEMENT NUMBER	
6. AUTHOR(S) Wendy L. Sarney			5d. PROJECT NUMBER 3NE6BB	
			5e. TASK NUMBER	
			5f. WORK UNIT NUMBER	
7. PERFORMING ORGANIZATION NAME(S) AND ADDRESS(ES) U.S. Army Research Laboratory Sensors & Electron Devices Directorate (ATTN: AMSRL-SE-EI) wsarney@arl.mil			8. PERFORMING ORGANIZATION REPORT NUMBER ARL-TR-3128	
9. SPONSORING/MONITORING AGENCY NAME(S) AND ADDRESS(ES) U.S. Army Research Laboratory 2800 Powder Mill Road Adelphi, MD 20783-1145			10. SPONSOR/MONITOR'S ACRONYM(S)	
			11. SPONSOR/MONITOR'S REPORT NUMBER(S)	
12. DISTRIBUTION/AVAILABILITY STATEMENT Approved for public release; distribution unlimited.				
13. SUPPLEMENTARY NOTES				
14. ABSTRACT Materials analysis is enhanced by transmission electron microscopy (TEM) images and their corresponding diffraction pattern data. While TEM images are widely reported and largely understood, the diffraction pattern data tends to be underused or completely neglected. Diffraction patterns complement TEM images by allowing accurate structural assessments, including lattice plane identification and defect characterization. This paper explains how to 'read' diffraction patterns by understanding how they relate to the crystal in real space. For ease of illustration we use examples from semiconductor materials grown for infrared detector research at ARL.				
15. SUBJECT TERMS Semiconductors, microanalysis, transmission electron microscopy				
16. Security Classification of:			17. LIMITATION OF ABSTRACT SAR	18. NUMBER OF PAGES 23
a. REPORT UNCLASSIFIED	b. ABSTRACT UNCLASSIFIED	c. THIS PAGE UNCLASSIFIED		
			19b. TELEPHONE NUMBER (Include area code) (301) 394-5761	

Standard Form 298 (Rev. 8/98)
Prescribed by ANSI Std. Z39.18

Contents

1. Introduction	1
2. FCC materials: Crystallography and reciprocal space	1
3. The crystal structure factor and allowed diffraction spots	4
4. Relationship between sample preparation and the diffraction pattern	6
5. Examples from ARIL projects	7
5.1 II-VI Semiconductor Films	7
5.2 III-V Semiconductor Films	14
6. Conclusion	15
7. Acknowledgment	16
8. References	16

List of Figures

Figure 1. Schematic of the zinc blende crystal structure in real space.	2
Figure 2. Schematic of the reciprocal lattice of the fcc crystal structure.	3
Figure 3. Low-index diffraction patterns for fcc crystals examined along the (a) $[1\bar{1}1]$, (b) $[100]$, (c) $[\bar{1}11]$, and (d) $[\bar{2}12]$ zone axes.	5
Figure 4. Basic TEM sample preparation process. (a) Wafer with film grown onto the substrate. (b) Sample is cleaved, and (c) polished to electron transparency. (d) Final crystallographic orientation of the specimen in the TEM. (e) Diffraction pattern obtained from this sample, the dashed lines represent the objective lens aperture.	6
Figure 5. (a) TEM diffraction pattern of Si taken from a sample having a $[111]$ growth direction. (b) A corresponding schematic of (a) showing the spot indices. (c) Resulting diffraction pattern when a $[110]$ Si diffraction pattern (Fig. 5a) is tilted along the $[002]$ axis.	8
Figure 6. Diffraction pattern taken at the interface of a ZnTe film grown on Si.	9
Figure 7. (a) Diffraction pattern of a Si substrate having a $[113]$ growth direction. (b) Diffraction pattern of a ZnTe film having a $[111]$ growth direction. (c) Diffraction pattern obtained at the ZnTe/Si interface.	9
Figure 8. High resolution image of a ZnTe/Si interface.	10
Figure 9. (a) Diffraction pattern of a Si substrate having a $[113]$ growth direction. (b) Diffraction pattern of the ZnTe film.	11
Figure 10. Schematic of a crystal and its twin.	11
Figure 11. Schematic of the ZnTe diffraction pattern from (a) the parent crystal A, (b) the twin of the parent crystal B, and (c) regions A and B.	12
Figure 12. High resolution image of a ZnTe film grown on Si. Regions labeled with an A refer to the parent crystal and regions labeled with a B refer to the twin of the parent crystal.	13
Figure 13. ZnTe film have twins across the (111) plane.	14
Figure 14. Diffraction pattern of a ZnTe film that has twins across the (111) plane (b) Diffraction pattern from parent crystal A and (c) region B, its twin across the (111) plane.	14
Figure 15. Diffraction pattern from a superlattice consisting of InAs quantum dots and GaAs buffer layers.	15

1. Introduction

One advantage of TEM over scanning electron microscopy (SEM) or visible light microscopy is the ability to obtain diffraction patterns from the specimen under observation. Diffraction patterns provide structural details related to the specimen's orientation, polytype, phase, and defect morphology. Diffraction pattern analysis is an excellent complement to x-ray diffraction data. Unfortunately, many researchers do not know how to extract information from diffraction patterns. It is common practice for scientific journal publications to include numerous TEM images without any reference to their corresponding diffraction pattern data. TEM images look like visible light images, although they are formed very differently and cannot be interpreted in the same manner. Diffraction patterns and information, however, are more abstract since they involve thinking in reciprocal space. Most scientists understand and trust x-ray diffraction data.

For this reason a microscopist will often accompany the TEM images with x-ray diffraction data, even when the same information could be obtained with TEM diffraction.

In the Electro-optics and Photonics division at the Army Research Laboratory (ARL) we grow and analyze semiconductor materials for infrared device applications. These materials include III-V alloys based on GaAs, InAs, InP and the antimonides, and II-VI CdTe based alloys. This report discusses how TEM diffraction data can reveal important structural characteristics of materials grown by molecular beam epitaxy (MBE) at ARL.

2. FCC materials: Crystallography and reciprocal space

All crystals have both a real and reciprocal lattice. The real lattice consists of an array of points that corresponds to the position of atoms in the crystal's unit cell. The reciprocal lattice also consists of an array of points, with each point corresponding to a set of planes within the crystal.

Many semiconductor materials form in the zinc blende crystal structure, as shown in Figure 1. This structure consists of two interpenetrating face-centered cubic (fcc) lattices displaced by $1/4$ of the length of the unit cell's diagonal. In a binary AB alloy (such as GaAs), all of the 'A' atoms will lie on one of the fcc lattices, while all of the 'B' atoms lie on the second fcc lattice. The zinc blende structure has ABAB stacking along the [111] direction. The structure is described in real space by its primitive translation vectors, which for an fcc lattice are:

$$\begin{aligned}\vec{a}_1 &= \frac{1}{2}a(\hat{y} + \hat{z}) \\ \vec{a}_2 &= \frac{1}{2}a(\hat{x} + \hat{z}), \\ \vec{a}_3 &= \frac{1}{2}a(\hat{x} + \hat{y})\end{aligned}\tag{1}$$

where a is the lattice constant of the unit cell.

The diffraction pattern contains all vectors normal to the reflecting planes in the specimen. These *reciprocal lattice vectors*, denoted as \vec{g} , have a magnitude equal to the reciprocal of their corresponding reflecting plane. A plane lying in a cubic coordinate system is system in is described by three indices denoted as h , k , and l . The indices are found by identifying where the plane intercepts the three axes of the coordinate system. The intercepts are quantified in terms of the crystal's lattice constants along these three directions. Next, take the reciprocal of these three numbers and reduce them to the smallest three integers having the same ratio. For cubic crystals, the relationship between the reciprocal lattice vector and the plane indices h , k , and l is

$$|\vec{g}| = \frac{1}{d_{hkl}} = \frac{\sqrt{h^2 + k^2 + l^2}}{a} \quad (2)$$

where d_{hkl} is the lattice spacing.

A crystal's reciprocal lattice vectors are expressed as

$$\vec{g} = v_1\vec{b}_1 + v_2\vec{b}_2 + v_3\vec{b}_3$$

where v_1 , v_2 , and v_3 are integers and \vec{b}_1 , \vec{b}_2 , and \vec{b}_3 are the primitive vectors of the reciprocal lattice. These axis vectors \vec{b} are related to the crystal's real space primitive lattice vectors \vec{a} by the relationship:

$$\begin{aligned} \vec{b}_1 &= 2\pi \frac{\vec{a}_2 \times \vec{a}_3}{\vec{a}_1 \cdot \vec{a}_2 \times \vec{a}_3} \\ \vec{b}_2 &= 2\pi \frac{\vec{a}_3 \times \vec{a}_1}{\vec{a}_1 \cdot \vec{a}_2 \times \vec{a}_3} \\ \vec{b}_3 &= 2\pi \frac{\vec{a}_1 \times \vec{a}_2}{\vec{a}_1 \cdot \vec{a}_2 \times \vec{a}_3} \end{aligned} \quad (3)$$

where x denotes the cross product.

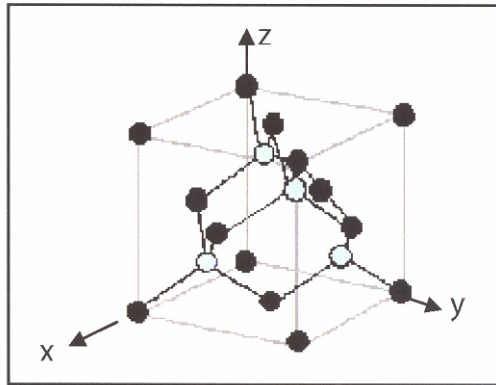


Figure 1. Schematic of the zinc blende crystal structure in real space.

By applying the fcc primitive lattice vectors (Eq. 1) to Eq. 3, we find that the reciprocal lattice vectors of the fcc lattice are:

$$\begin{aligned}\vec{b}_1 &= \frac{2\pi}{a}(-\hat{x} + \hat{y} + \hat{z}) \\ \vec{b}_2 &= \frac{2\pi}{a}(\hat{x} - \hat{y} + \hat{z}).\end{aligned}\tag{4}$$

The reciprocal lattice vectors of the fcc lattice (Eq. 4) are shown schematically in Figure 2.

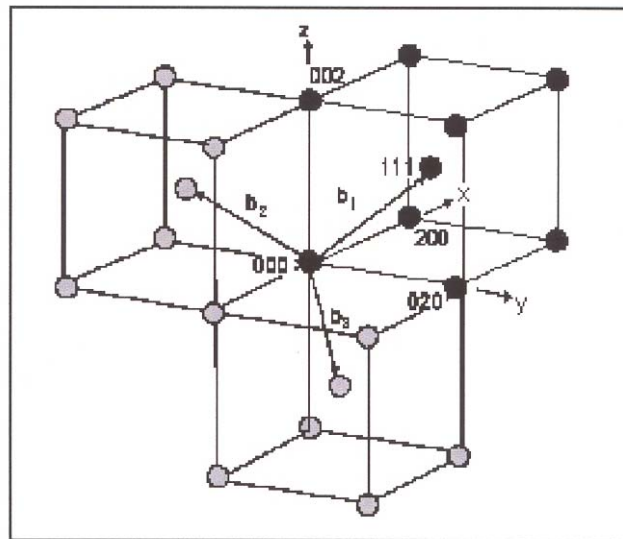


Figure 2. Schematic of the reciprocal lattice of the fcc crystal structure.

3. The crystal structure factor and allowed diffraction spots

The structure factor of a crystal is defined by the relationship

$$F_{hkl} = \sum_j f_j e^{2\pi i(hx_i + ky_i + lz_i)}, \quad (5)$$

which is the sum of the atomic scattering amplitudes from each of the i atoms in the unit cell (f_i) multiplied by a phase factor that accounts for the phase difference between waves scattered from atoms on different (hkl) planes [1]. The structure factor is the Fourier transform of the electron density of a crystal's unit cell. For a binary alloy AB with a zinc blende crystal structure, the basis consists of the A atoms located on the fcc lattice and the B atoms are displaced by $\frac{1}{4}$ of a unit cell diagonal from the A atoms. Substitution of the coordinates (x_i , y_i , and z_i) of the A and B atoms into Eq. 5 leads to

$$F = f_A \left(1 + e^{\pi i(h+k)} + e^{\pi i(k+l)} + e^{\pi i(h+l)} \right) + f_B \left(e^{\frac{\pi i}{2}(h+k+l)} + e^{\frac{\pi i}{2}(h+3k+3l)} + e^{\frac{\pi i}{2}(3h+k+3l)} \right). \quad (6)$$

Further simplification of Eq. 6 results in Eq. 7.

$$F = \{f_A + f_B e^{\frac{\pi i}{2}(h+k+l)}\} \cdot \{1 + e^{\pi i(h+k)} + e^{\pi i(h+l)} + e^{\pi i(k+l)}\}. \quad (7)$$

We then determine F for all hkl indices:

$$\begin{aligned} F &= 0 && \text{if } h, k, \text{ and } l \text{ are a mix of even and odd integers.} \\ F &= 4(f_A \pm if_B) && \text{if } h, k, \text{ and } l \text{ are all odd integers.} \\ F &= 4(f_A - f_B) && \text{if } h, k, \text{ and } l \text{ are all even integers and } h+k+l=2N \text{ where } N \text{ is odd.} \\ F &= 4(f_A + f_B) && \text{if } h, k, \text{ and } l \text{ are all even integers and } h+k+l=2N \text{ where } N \text{ is even.} \end{aligned} \quad (8)$$

The relationship between the scattering intensity I and the structure factor F is $I = |F|^2$. Therefore, F must be nonzero in order for diffraction spots to appear. Using Eq. 8, we find that the lowest index diffraction spots for a zinc blende crystal include 002, 111, and 220.

The distance between a diffraction spot and the transmitted beam spot (the large spot in the middle of the pattern) is defined by the relationship

$$R = \frac{\lambda L}{d_{hkl}}, \quad (9)$$

where λ is the wavelength of the electron beam, and L is the camera length (specific to the TEM). The geometric arrangement of the spots in the pattern relative to one another is easily determined with the definition of a dot product.

Figure 3 shows the four lowest index diffraction patterns that are observable for zinc blende materials. Each pattern is referred to by its 'one axis' which is defined as the direction perpendicular to all of the crystal planes that satisfy the Bragg condition. These planes are represented by the spots in the diffraction pattern. It therefore follows that the zone axis also specifies the direction of the incident electron beam with respect to the crystal. For illustrative purposes, examine Figure 3a, which shows a diffraction pattern having a zone axis (sometimes it is simply called a diffraction pattern). Notice that $[1\bar{1}0]$ is perpendicular to the normal of all of the (hkl) planes represented in the pattern (such as (002) , (111) , (220) , etc.).

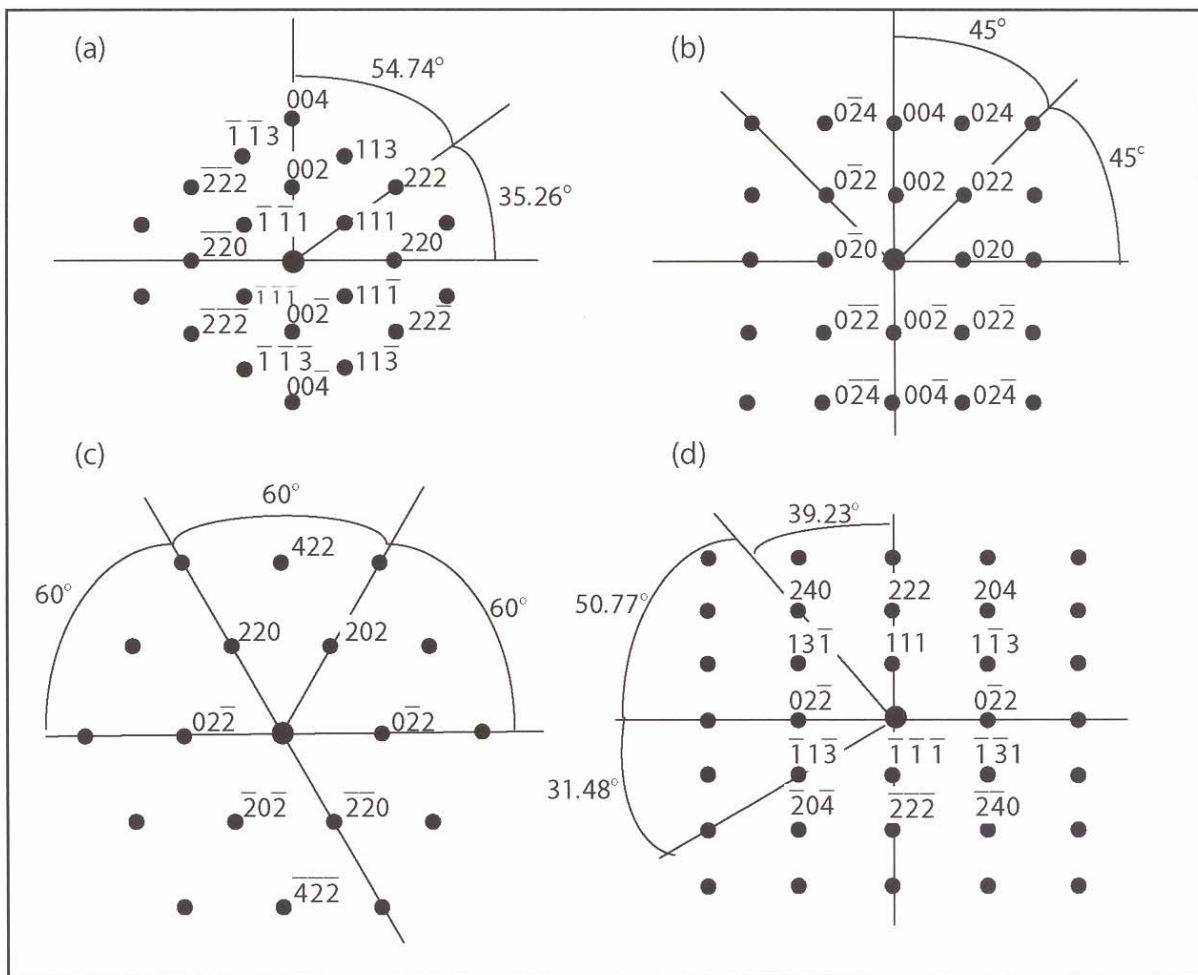


Figure 3. Low-index diffraction patterns for fcc crystals examined along the (a) $[1\bar{1}1]$, (b) $[100]$, (c) $[\bar{1}11]$, and (d) $[\bar{2}12]$ zone axes.

4. Relationship between sample preparation and the diffraction pattern

Samples are normally prepared so that the lowest index planes are observed. Most zinc blende films are prepared to allow the observation of the $[1\bar{1}0]$ zone axis. Figure 4 shows a very basic set of schematics demonstrating the sample preparation process. The wafer illustrated in Figure 4a has a (001) growth direction (this is typical for both the antimonide and InAs/GaAs quantum dot detector and laser structures). The sample is cleaved into a small rectangle having edges along the $\langle 110 \rangle$ -type directions (Figure 4b). We then polish and ion mill the sample until we obtain electron transparency along the $(1\bar{1}0)$ direction. The sample is placed into the TEM so that its $(1\bar{1}0)$ direction lies parallel to the electron beam. A sample oriented and prepared as shown in Fig 4a-d would have the diffraction pattern shown in Figure 4e.

As expressed in Eq. 9, the distance between a diffracted and transmitted spot is inversely proportional to the corresponding lattice spacing. Therefore, spots that are closer to the transmitted

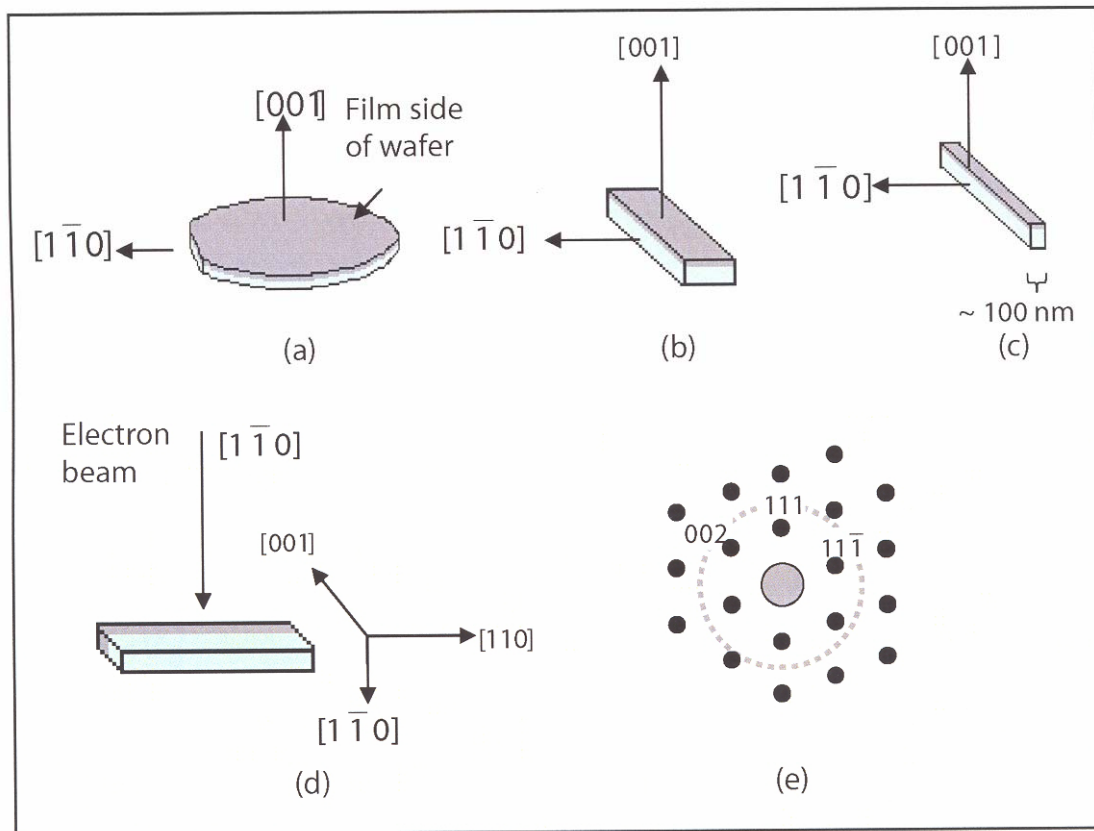


Figure 4. Basic TEM sample preparation process. (a) Wafer with film grown onto the substrate. (b) Sample is cleaved, and (c) polished to electron transparency. (d) Final crystallographic orientation of the specimen in the TEM. (e) Diffraction pattern obtained from this sample, the dashed lines represent the objective lens aperture.

beam correspond to larger lattice spacings, which are most likely to fall within the resolution limits of the TEM. High resolution images are obtained by placing an objective lens aperture around the first order diffraction spots. High resolution images obtained for an $[1\bar{1}0]$ incident electron beam would show lattice fringes corresponding to the (002), (111), and $(1\bar{1}1)$ planes. For GaAs, these planes correspond to lattice spacings of 2.8264 Å, 3.2639 Å, and 3.2639 Å respectively, which are within the resolution limits of a 200 kV TEM. By comparison, when the sample is oriented so that the electron beam is along the $(\bar{1}11)$ direction we obtain the diffraction pattern shown in Figure 4e. The nearest diffraction spots would correspond to the {202} crystal planes. This would require us to image planes having lattice spacings of 1.9987 Å. A well aligned 200 kV TEM would be able to image the (202) planes (but the image quality would likely be inferior to that obtained for the sample imaged along the $[1\bar{1}0]$ direction).

5. Examples from ARIL projects

5.1 II-VI Semiconductor Films

Many films are grown onto substrates with which they have a significant lattice mismatch. Sometimes the film and substrate have a crystal stacking mismatch (the substrate is then known as a nonisomorphic substrate). Growing films onto these types of substrates often leads to films with crystallographic defects that are apparent in TEM images and diffraction patterns. Common examples include III-V wide bandgap semiconductors such as GaN [1] and II-VI HgCdTe [2] semiconductors. An ongoing experiment at ARL involves growing CdTe layers on top of ZnTe buffer layers grown on Si substrates.

Si has the diamond crystal structure, which is identical to the zinc blende structure with the exception that each atomic site is populated by the same atom. Using Eq. 5, we find that the structure factor for Si is nearly the same as that for GaAs, the only major exception is that $F = 0$ for $h + k + l = 2N$, where N is odd. This means that the 002 reflection is now “forbidden.”

Figure 5 shows a $[1\bar{1}0]$ diffraction pattern taken from a Si substrate having a $[111]$ growth direction. Notice that this diffraction pattern is the same as that shown in Figure 3a (except that it is rotated by 54° since the growth direction is $[111]$ rather than $[002]$). Figure 5 shows that the (002) spot is clearly visible in spite of it not meeting structure factor rules.

Forbidden spots often occur due to multiple diffraction of the beam as it passes through the sample. Each diffracted beam can act as a pseudo-incident electron beam and be re-diffracted by

other planes. The (002) spot results when the incident $1\bar{1}0$ beam is diffracted by the (111) plane and then re-diffracted by the $(\bar{1}\bar{1}1)$ plane, as shown by vector addition

$$111 + \bar{1}\bar{1}1 = 002. \quad (10)$$

Some semiconductor films, such as SiC, have several polytypes. The appearance of forbidden spots in a diffraction pattern can cause polytype misidentification. In order to determine whether a spot is ‘real’ or the result of multiple-diffraction, the specimen must be tilted along the axis of the suspicious spot. In the case of the Si specimen (Figure 5a), if we tilt along the [002] axis, the 111 and $\bar{1}\bar{1}1$ spots lose intensity, and the 002 spot will disappear (Figure 5c). If the 002 spot was a ‘real’ allowed spot, it would remain visible despite our tilting the specimen.

Si and ZnTe have a lattice mismatch of 11%. By placing the selected area aperture (which isolates the specific area of the sample that will contribute to the diffraction pattern) over the Si/ZnTe interface, we obtain an overlay of the Si and ZnTe patterns (schematic shown in Figure 6). The ZnTe spots (denoted by the light gray circles) are located closer to the transmitted beam than the Si spots (denoted by the black circles), since ZnTe has a larger lattice constant (6.103 \AA) than Si (5.431 \AA).

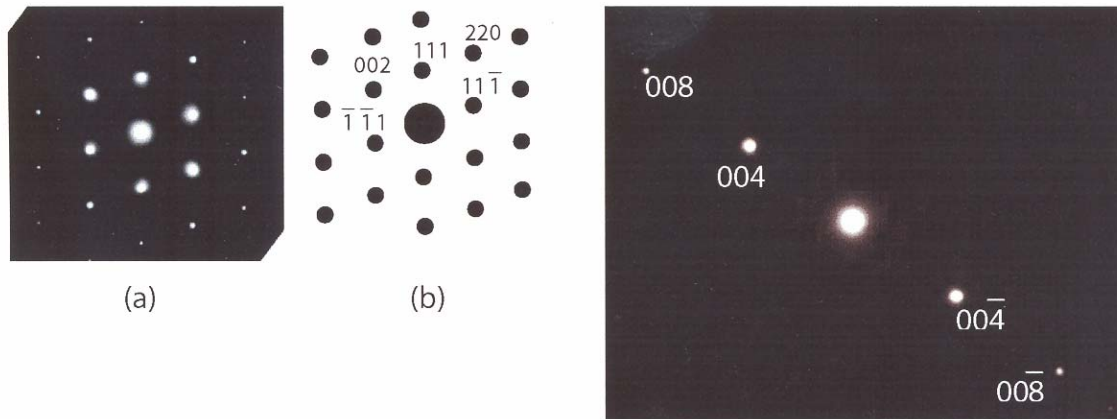


Figure 5. (a) TEM diffraction pattern of Si taken from a sample having a [111] growth direction. (b) A corresponding schematic of (a) showing the spot indices. (c) Resulting diffraction pattern when a $[1\bar{1}0]$ Si diffraction pattern (Fig. 5a) is tilted along the [002] axis.

The pattern shown in Figure 6 occurs when the Si substrate and film have the same orientation. When we grow ZnTe onto Si substrates having a $[113]$ growth direction, we obtain films with a $[111]$ growth direction. Figure 7(a) shows a schematic of the diffraction pattern obtained for a Si substrate having a $[113]$ growth direction. Figure 7(b) is a schematic of the pattern obtained for a ZnTe film having a $[111]$ growth direction. If we center our selected area aperture over the ZnTe/ Si interface, we obtain the diffraction pattern shown in Figure 7(c). We can see that Figure 8c is an overlay of the patterns in Figures 7(a) and 7(b). When an objective lens aperture is placed around the first order spots (shown by the dashed line in Figure 7c), and the TEM is placed in image mode, we obtain the image shown in Figure 8. We can identify the lattice planes in Figure 8 by comparing the image with the diffraction patterns in Figure 7, since the orientation of the pattern directly corresponds to that of the image. For instance, a straight line drawn between the transmitted beam spot and the 111 spot in the ZnTe diffraction pattern corresponds to the $[111]$

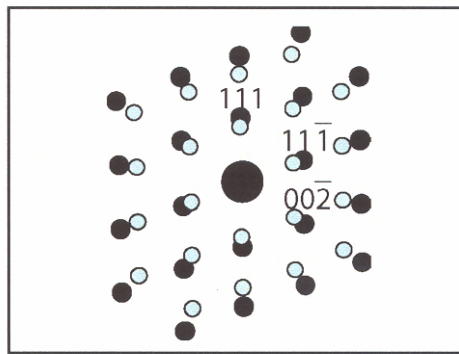


Figure 6. Diffraction pattern taken at the interface of a ZnTe film grown on Si.

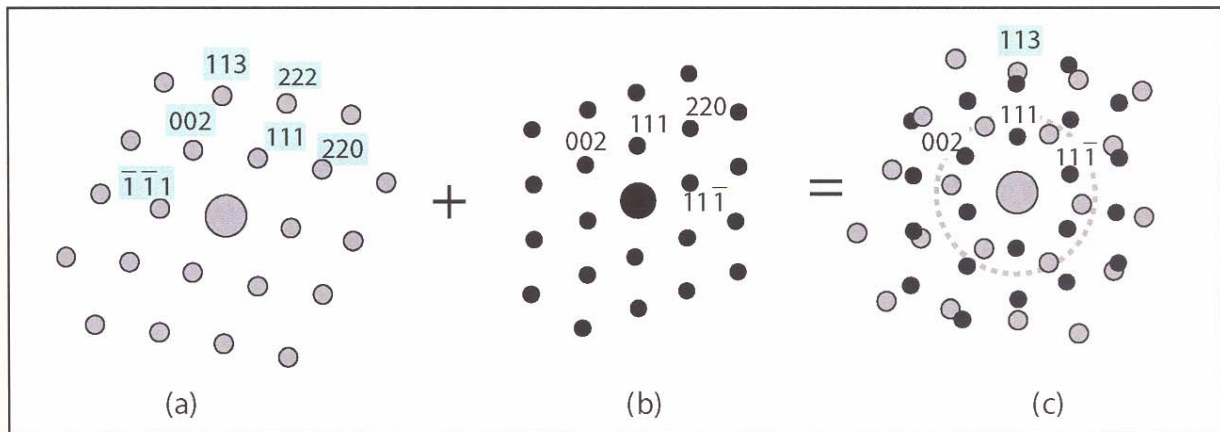


Figure 7. (a) Diffraction pattern of a Si substrate having a $[113]$ growth direction. (b) Diffraction pattern of a ZnTe film having a $[111]$ growth direction. (c) Diffraction pattern obtained at the ZnTe/Si interface.

direction in the image. The $\{111\}$ planes lie perpendicular to this line. The $\{111\}$, $\{11\bar{1}\}$, and $\{002\}$ planes are labeled in Figure 8. The lattice spacings can be directly measured from the image or from the diffraction pattern (with the help of Eq. 9). We find that the $d_{\text{ZnTe}}^{\{111\}}$ value measured from both the image and diffraction pattern directly agrees with $d_{\text{ZnTe}}^{\{111\}}$ calculated with Eq. 4 using the known value for the ZnTe lattice constant. For some semiconductor film/substrate systems we occasionally find that the measured value does not agree with that calculated from Eq. 4. The most common reason is due to the film being tetragonally distorted to accommodate strain. Another likely reason is because something other than the expected binary alloy has been deposited (usually because of an error in an MBE recipe resulting in the unexpected growth of a ternary). We can calculate strain by comparing the measured d for a film with the known d for bulk, unstrained material.

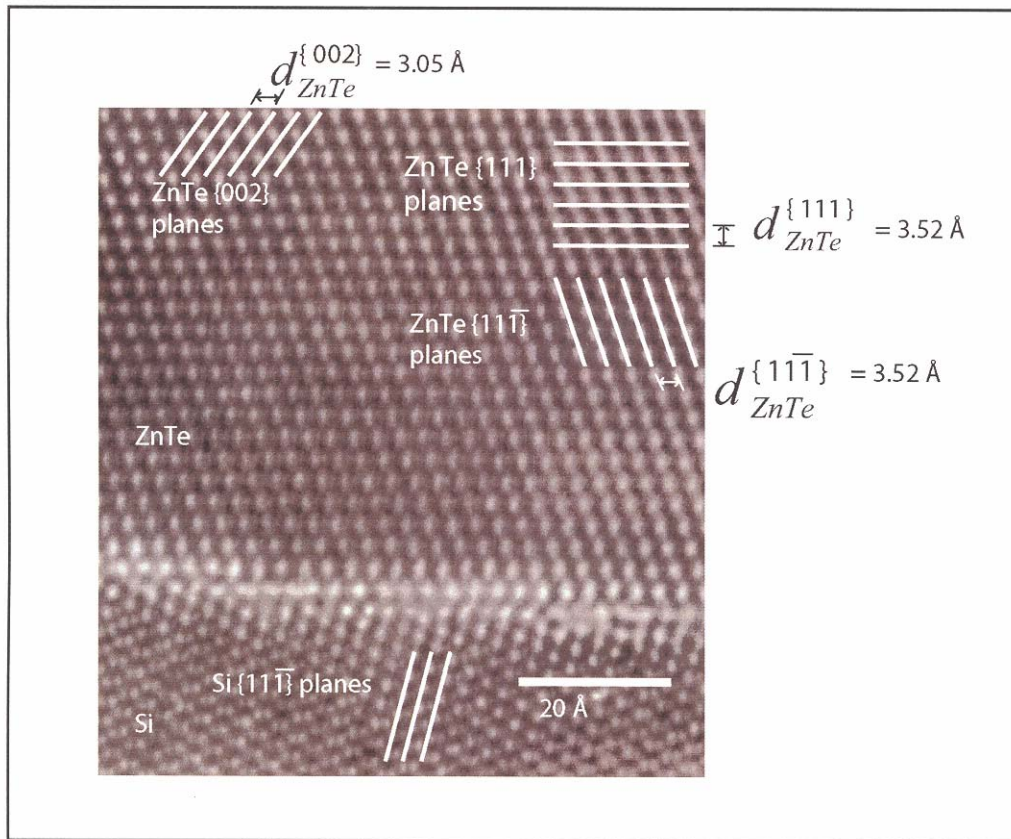


Figure 8. High resolution image of a ZnTe/Si interface.

In a recent experiment ZnTe was grown on a Si substrate having a [113] growth direction. The diffraction patterns of the substrate and the film are shown in Figures 9(a) and (b), respectively. The film was expected to have a [111] growth direction. When this sample was examined with x-ray, the grower was surprised to find that the {111} peaks were weaker than anticipated. At first glance the ZnTe film diffraction pattern (Figure 9b) does not look like any of the conventional fcc patterns shown in Figure 3. Whenever an unconventional diffraction pattern is obtained from a film that is expected to be crystalline, a microscopist must determine whether the irregularity is arising from either defects or the growth of an unintended crystal structure. In general, diffraction patterns containing rings of distinct spots result from film polycrystallinity. Diffraction patterns consisting of streaky rings usually indicate that a film has amorphous regions. A film may become amorphous due to growth problems, electron beam damage from the TEM, or damage from the sample preparation process.

Figure 9(b) shows a pattern of distinct spots with what may be a symmetry axis located 29.5° from the horizontal. These types of patterns often originate when a film contains twins, which are shown schematically in Figure 10.

Diffraction patterns are very useful for identifying twins in a film. Twinning is difficult to detect with x-ray; in fact, symmetric x-ray measurements can not detect twinning across some crystal planes. ZnTe films grown on Si having a <111> or <113> growth direction often contain high densities of twinned regions. The grower may be unaware of these twins, and become confused by the weakness of certain x-ray peaks or the presence of unexpected peaks.

Twinning is due to applied stresses within a crystal, which are often related to the lattice mismatch between a film and a substrate. The twinned portion of the crystal is a mirror image of the parent crystal. The twinned and untwinned regions have identical crystal structures, but the twinned region is misoriented across the twinning plane with respect to the parent crystal (Figure 10).

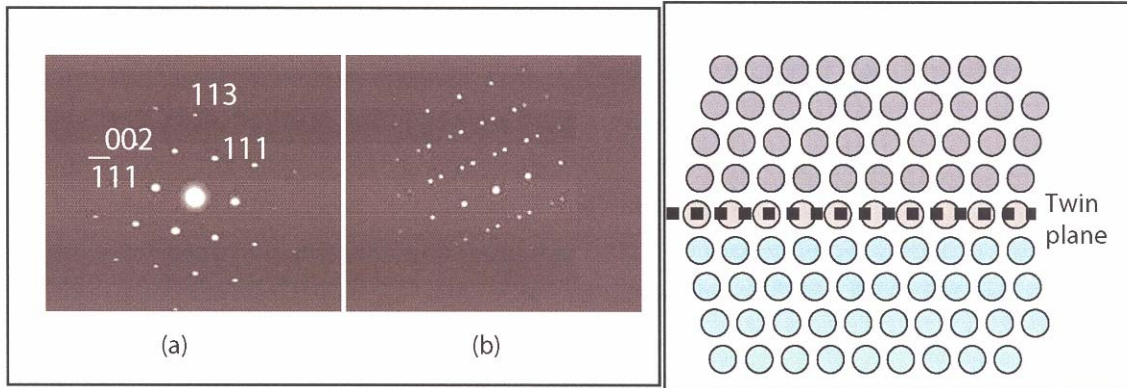


Figure 9. (a) Diffraction pattern of a Si substrate having a [113] growth direction. (b) Diffraction pattern of the ZnTe film.

Figure 10. Schematic of a crystal and its twin.

It is a relatively simple process to identify the unknown diffraction pattern in Figure 9b. We begin by drawing a schematic of the diffraction pattern obtained from a single crystal of ZnTe having a [111] growth direction (Figure 11 a). We will refer to the crystal that would generate this pattern as the parent crystal, or crystal 'A'. This is the diffraction pattern that we would expect if the entire film was single crystalline and had a [111] growth direction. We draw a dotted line with the same orientation as that of the suspected symmetry axis (Figure 9b). The line passes through the $11\bar{1}$ spot, indicating that the crystal may have twinning across the $(11\bar{1})$ plane. If we rotate the parent crystal's diffraction pattern 180° about the $(11\bar{1})$ plane, we obtain the pattern seen in Figure 11 b. Finally, if we superimpose the patterns in Figures 11 (a) and (b), we obtain the pattern shown in Fig 11 c. Notice that the schematic of Figure 11 c matches the diffraction pattern shown in Figure 9(b). Therefore, we conclude that the pattern shown in Figure 9B is obtained from a ZnTe film that has twinned regions across the $(11\bar{1})$ plane.

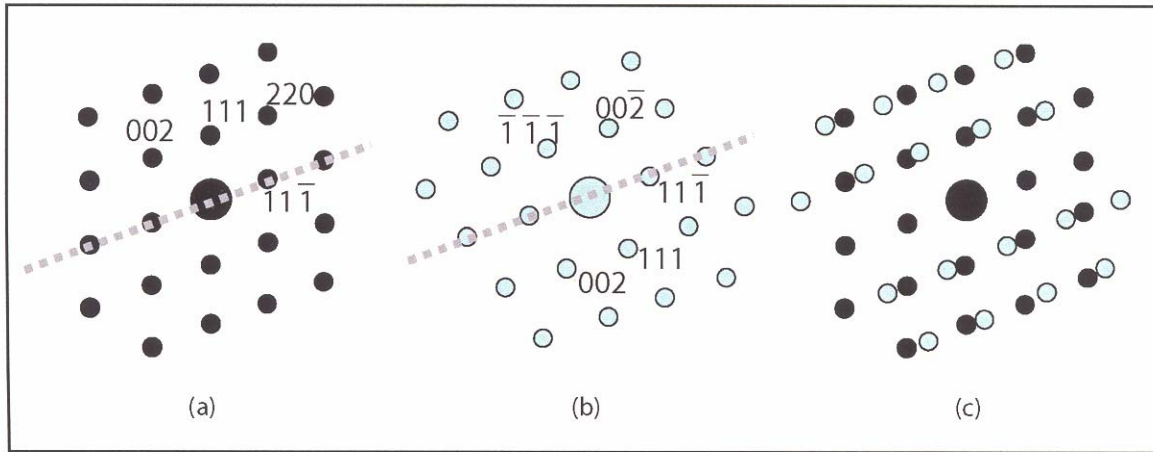


Figure 11. Schematic of the ZnTe diffraction pattern from (a) the parent crystal A, (b) the twin of the parent crystal B, and (c) regions A and B.

If we isolate the first order diffraction spots (Figure 9) with an objective lens aperture, we obtain the image shown in Figure 12. The regions labeled B, which are the mirror image of the parent crystal (A) across the $(1\bar{1}1)$ plane, give rise to the diffraction spots shown in Figure 11 b. The $\{111\}$ planes in B are rotated 39.1° counter-clockwise with respect to the (111) planes in A. Since a significant fraction of the sample contains twinned regions it follows that much of the film does not have the expected [111] growth direction. This would lead to a weaker [111] x-ray diffraction peak than expected. It would also lead to the presence of several peaks that correspond to planes in the twinned regions. For instance, if a film contains a sufficient density of 'B' regions (as shown in Figure 12), then the x-ray will detect a (111) peak located 39.1° from the (111) peak corresponding to the parent crystal.

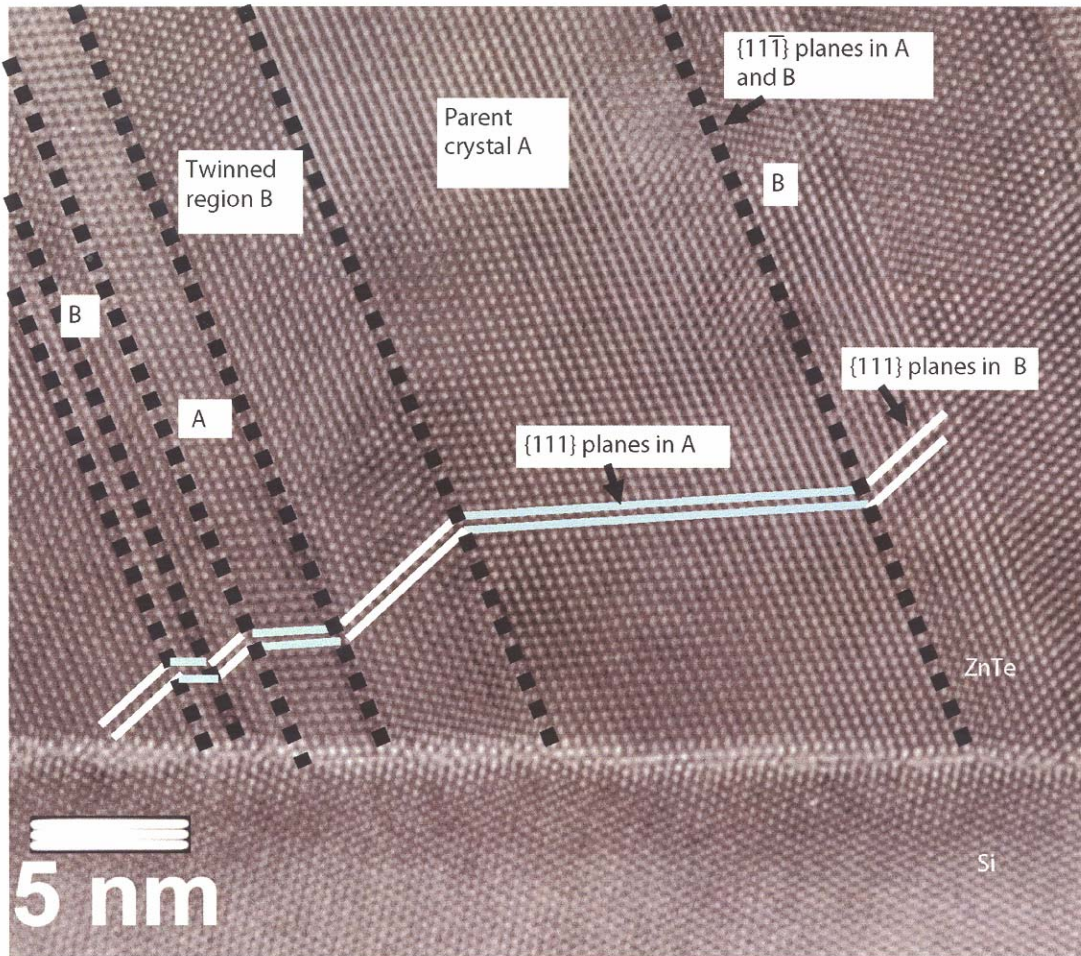


Figure 12. High resolution image of a ZnTe film grown on Si. Regions labeled with an A refer to the parent crystal and regions labeled with a B refer to the twin of the parent crystal.

Some types of twins may be completely undetected by symmetric x-ray scans. Figure 13 shows a TEM image of a ZnTe film that has twinning across the (111) plane. It is clear from this image that region B is the mirror image of the parent crystal A. Figure 14(a) is a schematic of the diffraction pattern obtained from the sample shown in Figure 13. The diffraction pattern of the parent crystal A is shown in Figure 14b. The pattern in Figure 14c is the mirror image (180° rotation about the (111) plane) of that shown in 14b. This type of twinning defect would not cause a distortion in the lattice spacing along the [111] growth direction. Also, the (111) planes in both regions A and B have the same orientation. Therefore, a simple symmetric x-ray study of the (111) planes would not detect any irregularities due to twinning across the (111) plane. It is very common for these types of x-ray scans to be done as first-level quality assessments of semiconductor wafers; however, that they are ‘blind’ to this type of twinning defect. Since twinning is a common problem in films having a (111) growth direction, it is critical that in-depth diagnostic assessments beyond basic x-ray are used when analyzing these types of structures.

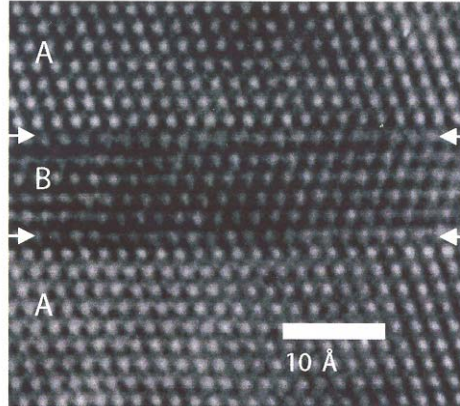


Figure 13. ZnTe film have twins across the (111) plane.

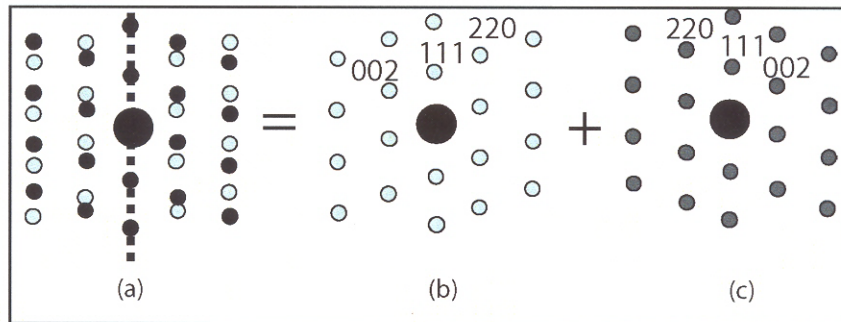


Figure 14. Diffraction pattern of a ZnTe film that has twins across the (111) plane (b) Diffraction pattern from parent crystal A and (c) region B, its twin across the (111) plane.

5.2 III-V Semiconductor Films

Many ARL projects involve depositing III-V semiconductor structures on GaAs, GaSb, InAs, or InP substrates. The substrates usually have a [001] growth direction, although occasionally substrates with a small miscut are used to minimize the film/substrate lattice mismatch. When viewed along the $[1\bar{1}0]$ zone axis, the diffraction pattern of single-crystalline III-V semiconductor materials with a [001] growth direction looks as shown in Figure 3a.

Figure 15 shows a diffraction pattern obtained from a superlattice consisting of InAs quantum dots and GaAs spacer layers grown onto a GaAs substrate. Notice that, unlike the diffraction pattern obtained from the ZnTe/Si system, there is only one set of spots for the InAs/GaAs system. The lattice mismatch between InAs and GaAs is 6.9% (compared with 11% for ZnTe/Si). Therefore, the distances between the InAs and GaAs spots corresponding to the same hkl plane are visually indistinguishable. The superposition of the InAs and GaAs diffraction patterns appear as one diffraction pattern.

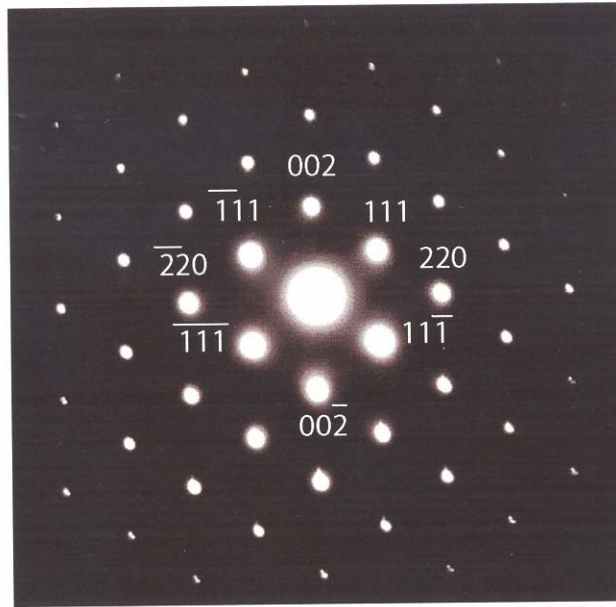


Figure 15. Diffraction pattern from a superlattice consisting of InAs quantum dots and GaAs buffer layers.

Commercial software exists that takes digitally collected diffraction patterns from the TEM and compares them with the expected diffraction patterns from a database. It can decipher precise shifts in spot position (that we can't measure with our eyes and a ruler on the TEM negative) and use this information to calculate the strain in the film. The software can also be used to identify the structure, polytype, and composition (such as the percentage of Al in an AlGaAs film) of a specimen.

We can generate TEM images of specific hkl planes by placing an objective lens aperture around an individual diffraction spot. This mode of operation is known as diffraction contrast imaging and is very useful for identifying defects and enhancing image contrast. Diffraction contrast imaging will be discussed in a future technical report.

6. Conclusion

Diffraction pattern analysis provides detailed structural information. This paper used several examples from both II-VI and III-V semiconductor films to demonstrate typical materials characterization that is accomplished with TEM diffraction patterns.

7. Acknowledgment

The author thanks Greg Brill for the MBE growth of the ZnTe/Si films and John Little for the MBE growth of the InAs quantum dot/GaAs films.

8. References

[1] Williams, David B. and Carter, C. Barry, *Transmission Electron Microscopy II*, Plenum Press, New York, p. 43, 1996.

[2] Lee, C. D., V Ramachandran, Ashutosh Sagar, R. M. Feenstra, D. W. Greve, W. L. Sarney, L. Salamanca-Riba, D. C. Look, Song Bai, W. J. Choyke, and R. P. Devaty "Properties of GaN epitaxial layers grown on 6H-SiC(0001) by plasma-assisted molecular beam epitaxy," *J Electronic Materials*, vol. 30, pp. 162-169, March, 2001.

[3] Brill, G., S. Velicu, P. Boieriu, Y Chen, N. K. Dhar, T. S. Lee, Y Selamet, and S. Sivananthan, "MBE growth and device processing of MWIR HgCdTe on large area Si substrates," *Journal of Electronic Materials*, vol. 30, no. 6, pp. 717-722, June 2001.

Distribution List

US Army Rsrch Lab

ATTN AMSRL-CI-IS-R Mail & Records Mgmt

ATTN AMSRL-CI-IS-T Techl Pub (2 copies)

ATTN AMSRL-CI-OK-TL Techl Lib

(2 copies)

ATTN AMSRL-SE-E G Simonis

ATTN AMSRL-SE-EI D Beekman

ATTN AMSRL-SE-EI J Little

ATTN AMSRL-SE-EI N Dhar

ATTN AMSRL-SE-RL S Svensson

ATTN AMSRL-SE-EI W Sarney (20 copies)